ACS Macro Letters

Letter

pubs.acs.org/macroletters

Three-Dimensional Periodically Ordered Nanohetero Metallic Materials from Self-Assembled Block Copolymer Composites

Hiroaki Wakayama,* Hirotaka Yonekura, and Yasuaki Kawai

Toyota Central R&D Laboratories, Inc., Nagakute, Aichi 480-1192, Japan

Supporting Information

ABSTRACT: We report a synthetic route to inorganic nanoheterostructures with tunable size and morphology via self-assembled block copolymer mesophase templates. Two Fe precursors, tricarbonyl(cyclooctatetraene) iron and acetylacetonate iron(III), and one Pt precursor, platinum dimethylcyclooctadiene, were selectively introduced into separate polymer blocks of a block copolymer, polystyrene-*b*-poly-4-vinylpyridine, and then the block copolymer templates were removed by pyrolysis. Self-assembled inorganic nanoheterostructures (spheres, hexagonal cylinders, and layers of hard magnetic phase FePt in a matrix of soft magnetic phase α-Fe) were produced. The morphology and domain size of the nanoheterostructures could be tailored by controlling the molecular weight and relative block lengths of the block copolymers. The controlled size and morphology of the inorganic nanoheterostructures demonstrate the method's utility for producing highly functional materials.

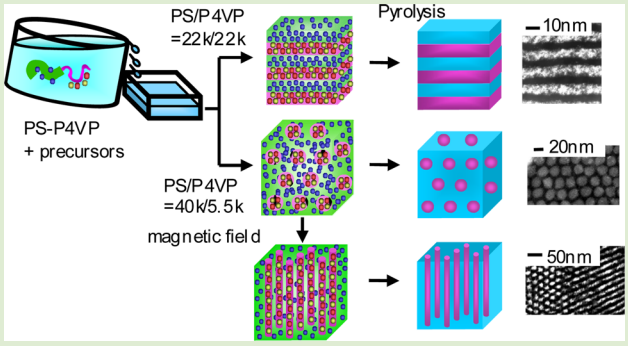

Inorganic nanoheterostructures offer great promise owing to their unique electronic,[1,2] ionic,[3] magnetic,[4−7] and photonic[8,9] properties. For example, in permanent magnetic applications, periodically ordered inorganic nanoheterostructures containing magnetically hard and soft phases with controlled size and morphology are important owing to the high magnetic performance of such structures.[4−6] However, the realization of practical applications of these structures will require control of their size and morphology with periodicity on a scale of <100 nm. Periodically ordered inorganic nanoheterostructures have been prepared by layer-by-layer adsorption,[10] sputtering,[11] and self-assembly methods.[12] However, most of the structures fabricated to date have been limited to layered materials. Phase separation (e.g., spinodal decomposition) induced by heat treatment is commonly used to control metal texture on the nanometer scale, but periodically ordered nanoheterostructures are not formed in the phase-separated materials produced by this method. Metallosupramolecular polymers offer an interesting platform for in situ formation of metal nanoparticles in polymer matrices to yield uniformly sized, unagglomerated nanoparticles[13] or metallic nanolines by polymer nanoimprint lithography.[14]

Self-assembly processes are advantageous for nanostructure fabrication because they consume less energy than conventional nanotechnology processing does. The synthesis of nanostructured inorganic materials from self-assembled block copolymer (BCP) mesophases is a fascinating method that allows control of size and shape.[15−24] Mesoporous structures,[15−17] inorganic nanoparticles of various shapes,[18−20] and arrays of cylinders[21,22] can be produced from BCP mesophases by selectively introducing precursors into one polymer block of BCPs or by using covalent ligation into a polymer block[23,24] and then removing the BCPs. The nanostructures produced by these methods are replicates of only one polymer block. Although nanoparticles decorated with organic ligands can be introduced into specific polymer blocks or the interface between polymer blocks,[25] the introduction of many nanoparticles into phase-separated BCP structures results in nanoparticle aggregation, which inhibits self-assembly.[26] There has been only limited research on the fabrication of inorganic nanoheterostructures by replication of two polymer blocks into which precursors or nanoparticles have been introduced separately,[27] and the reported structures obtained by this route consist of a single monolayer on a substrate. The three-dimensional replication of ordered BCP morphologies by selective introduction of inorganic precursors into two polymer blocks remains a great challenge.

Herein, we present a simple method for producing three-dimensional periodically ordered inorganic nanoheterostructures with controlled shape and size by replicating two polymer blocks of self-assembled BCPs containing metal precursors. Two Fe precursors and one Pt precursor were dissolved with BCPs in a solvent. Upon evaporation of the solvent, each precursor was selectively introduced into a separate polymer block. Subsequent pyrolytic removal of the BCPs produced periodically ordered nanoheterostructures that were structural replicates of the precursor−BCP composites.

Received: December 6, 2012
Accepted: March 11, 2013
Published: March 15, 2013

   dx.doi.org/10.1021/mz300634p | *ACS Macro Lett.* 2013, 2, 284−287

The two Fe precursors, tricarbonyl(cyclooctatetraene) iron [$CtFe(CO)_3$] and acetylacetonate iron(III) [$Fe(acac)_3$], were dissolved, along with the Pt precursor, platinum dimethylcyclooctadiene [$PtMe_2COD$], in a toluene solution containing the BCP polystyrene-*b*-poly-4-vinylpyridine (PS-P4VP, where the PS/P4VP molecular weight ratio was 22k/22k or 40k/5.5k), and the solution was transferred to a Petri dish (Figure 1a). BCP−precursor composites were produced at PS/P4VP = 22k/22k and 40k/5.5k to generate two different mesophases (Figure 1b,c). Specifically, upon evaporation of the solvent, the Fe precursors (brown and blue spheres) were introduced into both the PS block and the P4VP block, whereas the Pt precursor (red spheres) was introduced preferentially into the P4VP block. The PS-P4VP BCPs and the three precursors coassembled into either lamellae or spheres in a matrix, depending on the PS/P4VP molecular weight ratio. The formation of the latter morphology was driven by the selective dissolution of the PS block in toluene,[28] which resulted in the dissolution of the Pt and Fe precursors (red and yellow spheres) in P4VP spheres (larger pink spheres) embedded in a PS matrix (green) containing additional Fe precursors (blue spheres; Figure 1c). Application of an external magnetic field (10 T) to the PS-P4VP (40k/5.5k)−precursor composites at 453 K resulted in a phase transition of the P4VP block from spheres to hexagonal cylinders (Figure 1d). After the removal of the BCPs by pyrolysis, periodically ordered inorganic nanoheterostructures, templated by the self-assembled precursor−BCP composites, were obtained (Figure 1e−g). The lamellar, spherical, and hexagonal cylindrical structures of the precursor−BCP composites were preserved in the periodically ordered nanoheterostructures as inorganic layers, spheres, and cylinders (purple), respectively, embedded in an inorganic matrix (light blue).

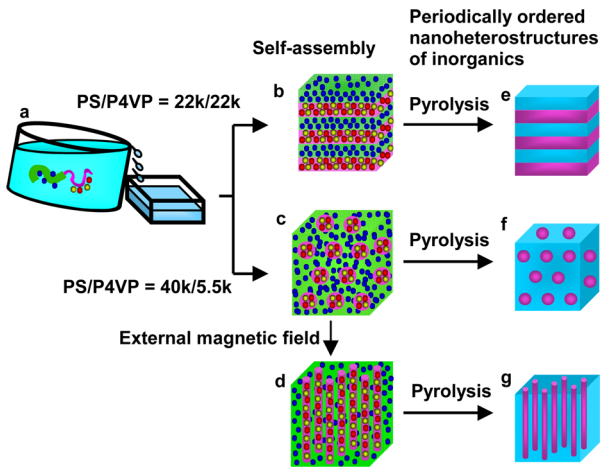

Figure 1. Preparation of periodically ordered inorganic nanoheterostructures from self-assembled block copolymer composites. (a) Dissolution of PS-P4VP block copolymers (PS, green; P4VP, pink) and Fe (brown and blue spheres) and Pt (red spheres) precursors. (b) Self-assembly of a lamellar structure from PS-P4VP (22k/22k) and precursors. (c) Self-assembly of a spheres-in-a-matrix structure (P4VP spheres, pink; PS matrix, green) from PS-P4VP (40k/5.5k) and precursors. (d) Self-assembly of hexagonal cylinders upon application of a magnetic field to sample shown in panel (c). Pyrolytic formation of periodically ordered nanoheterostructures consisting of (e) layers, (f) spheres, and (g) cylinders (purple) embedded in a matrix (light blue).

Analysis of small-angle X-ray scattering (SAXS) patterns revealed that the relative positions of the 1:2:3, $1:\sqrt{2}:\sqrt{3}:\sqrt{4}$, and $1:\sqrt{3}:\sqrt{4}:\sqrt{7}$ peaks confirmed lamellar (Figure 2a,b),

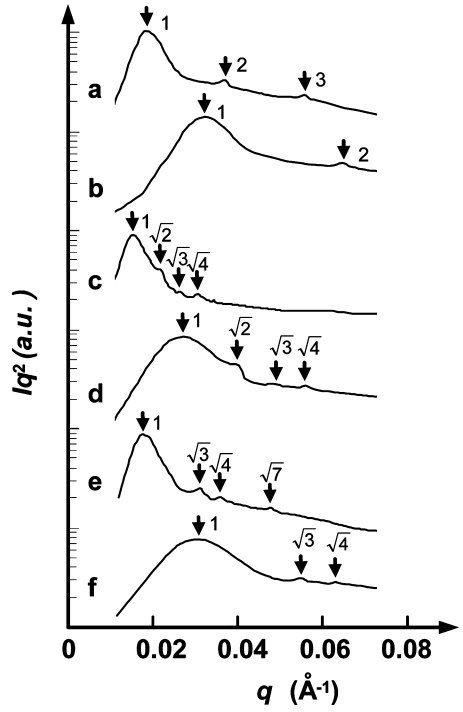

Figure 2. SAXS profiles of (a) a BCP−precursor composite prepared from PS-P4VP (22k/22k) and (b) the same sample after pyrolysis; (c) a BCP−precursor composite prepared from PS-P4VP (40k/5.5k) and (d) the same sample after pyrolysis; and (e) a BCP−precursor composite prepared from PS-P4VP (40k/5.5k) and subjected to a magnetic field and (f) the same sample after pyrolysis.

spherical (Figure 2c,d), and hexagonal cylindrical (Figure 2e,f) structures, respectively. Pyrolysis of the BCP−precursor composites was accompanied by decreases in the (1, 0) *d*-spacings from 31.5, 39.1, and 33.5 nm to 18.1, 21.5, and 19.1 nm for the lamellar, spherical, and hexagonal cylindrical samples, respectively. These results show that the nanostructures of the self-assembled BCP−precursor composites were retained in the samples after BCP removal.

The energy-dispersive spectrometry (EDS) map of a BCP−precursor composite sample produced from the three precursors (Figure S1b,c, Supporting Information) suggests that the Fe precursors were introduced into both the PS block and the P4VP block, whereas the Pt precursor was introduced preferentially into the P4VP block. In comparison, in a sample produced with only one Fe precursor [$Fe(acac)_3$] and the Pt precursor, the Fe precursor was introduced preferentially into the P4VP block (Figure S2b, Supporting Information). These results suggest that $Fe(acac)_3$ and $CtFe(CO)_3$ were introduced preferentially into the P4VP and PS blocks, respectively. The SAXS profile of the PS/P4VP (40k/5.5k) sample exposed to an external magnetic field of 10 T at 453 K shows that application of the field transformed the P4VP spheres to hexagonal cylinders (Figure 2c,e). It is suggest that the interaction between the interface of the two polymer blocks and the magnetic field induced the phase transition from spheres to cylinders and the preferential orientation of cylinder microdomains.[29] Metal precursors would enhance this effect.

dx.doi.org/10.1021/mz300634p | *ACS Macro Lett.* 2013, 2, 284−287

Scanning transmission electron microscopy (STEM) images of the pyrolyzed samples show that the self-assembled lamellar, spherical, and hexagonal cylindrical structures were preserved after removal of the BCPs (Figure 3a–c), confirming the SAXS

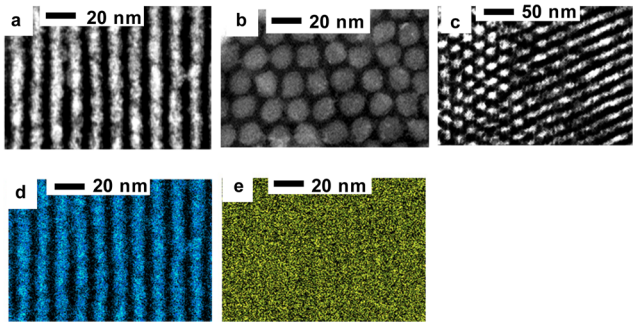

Figure 3. Dark-field STEM images of pyrolyzed samples prepared at (a) PS/P4VP = 22k/22k and (b) PS/P4VP = 40k/5.5k; (c) STEM image of the sample in panel (b) after a magnetic field was applied; EDS mapping images for (d, blue) Pt and (e, green) Fe after pyrolysis of the sample in panel (a).

results. A dark-field STEM image of the local structure of a pyrolyzed sample prepared at PS/P4VP = 22k/22k shows a lamellar morphology, with the bright areas in the image corresponding to more-electron-dense layers (Figure 3a). The EDS map of the local structure clearly shows that Pt was homogeneously distributed in the region of more-electron-dense layers in the STEM image (Figure 3d). In contrast, Fe was located in both the bright region and the dark region (Figure 3e). These results indicate that the nanostructure of the pyrolyzed sample prepared at PS/P4VP = 22k/22k was composed of alternating Fe and Pt/Fe lamellae. There was a small amount of residual carbon (6 wt%, as indicated by inductively coupled plasma atomic emission spectrometry) in the pyrolyzed sample.

The thermogravimetric analysis curve for the pyrolyzed sample prepared at PS/P4VP = 22k/22k exhibited weight loss up to 480 K (Figure S5a, Supporting Information), indicating that the metal precursors decomposed in this temperature range. Additional weight loss occurs from 640 to 730 K due to decomposition of the BCP in the composite sample; this temperature range corresponded to the temperature range for the complete decomposition of BCP alone. The ceramic yield calculated from the thermogravimetric analysis result was 33%.

We also used polystyrene-*b*-poly-2-vinylpyridine (PS-P2VP) BCPs with various molecular weights to control the size of the self-assembled nanoheterostructures. Dark-field STEM images of BCP–precursor composite samples and corresponding EDS Pt and Fe mapping images suggested that the Fe precursors were introduced into both the PS and the P2VP blocks, whereas the Pt precursor was introduced preferentially into the P2VP block (Figure S3, Supporting Information). Formation of lamellar BCP–precursor composite mesophases was confirmed. As the molecular weight of PS-P2VP was increased from 80.5 to 265 kg/mol, the repeat distance of the lamellar structure increased from 36 to 60 nm before pyrolysis and from 20 to 34 nm after pyrolysis (Figure 4). These results demonstrate that the domain size of the self-assembled nanoheterostructures before and after removal of the BCP templates could be tailored by changing the molecular weight of the BCPs.

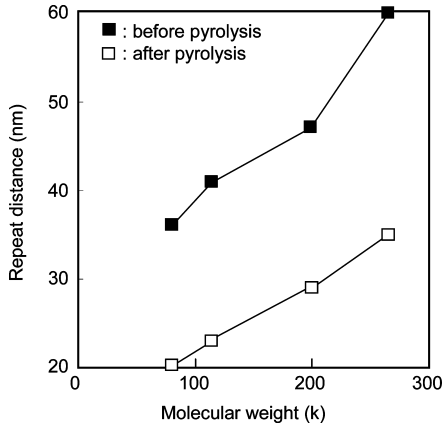

Figure 4. BCP-molecular-weight dependence of the repeat distance of the lamellar structure of a BCP–precursor composite sample produced from PS-P2VP.

The wide-angle X-ray scattering profile of the pyrolyzed sample prepared at PS/P4VP = 22k/22k confirmed the existence of two crystalline phases (Figure S4, Supporting Information). One phase was identified as the $L1_0$ tetragonal hard magnetic phase, corresponding to isotropic FePt. The other phase was the α-Fe phase, which is a soft magnetic phase with a large saturation magnetization.

In summary, we have demonstrated a powerful wet self-assembly process for preparing three-dimensional periodically ordered inorganic nanoheterostructures with tunable sizes and morphologies. This process may be applicable to other chemical species, such as other metals, oxides, carbides, nitrides, and sulfides, and can be expected to permit the mass production of periodically ordered inorganic nanoheterostructures over large areas or in bulk molding. Furthermore, the process requires minimal energy, involving simple mixing of the precursors and BCPs in solution and subsequent pyrolysis. This process provides a platform from which novel nanostructured materials can be prepared.

■ EXPERIMENTAL SECTION

In a typical preparation procedure, tricarbonyl (cyclooctatetraene) iron ($CtFe(CO)_3$, Tokyo Chemical Industry, >96%), dimethyl(1,5-cyclooctadiene) platinum(II) ($PtMe_2COD$, Wako Pure Chemical Industries, 99%), and acetylacetonate iron(III) ($Fe(acac)_3$, Wako, 99%) were dissolved in a 0.5 wt % solution of polystyrene-*b*-poly(4-vinylpyridine) (PS-P4VP, Polymer Source, M_n^{PS} = 22 kg mol^{-1}, M_n^{P4VP} = 22 kg mol^{-1}, polydispersity index =1.09) in toluene (Wako, >99.5%). The $CtFe(CO)_3$/styrene, $PtMe_2COD$/vinylpyridine (VP), and $Fe(acac)_3$/VP molar ratios were 1.0, 0.5, 0.5, respectively. After stirring, the solution was transferred to a Petri dish. The samples were pyrolyzed at 823 K for 6 h under a flow of H_2 in Ar. In some of the experiments, PS-P4VP (40k/5.5k; Polymer Source, M_n^{PS} = 40 kg mol^{-1}, M_n^{P4VP} = 5.5 kg mol^{-1}, polydispersity index = 1.09) was used in place of the PS-P4VP (22k/22k). We also used PS-P2VP (Polymer Source, M_n^{PS} = 40.5 kg mol^{-1}, M_n^{P2VP} = 40 kg mol^{-1}, polydispersity index = 1.10), PS-P2VP (Polymer Source, M_n^{PS} = 57 kg mol^{-1}, M_n^{P2VP} = 57 kg mol^{-1}, polydispersity index =1.10), PS-P2VP (Polymer Source, M_n^{PS} = 102 kg mol^{-1}, M_n^{P2VP} = 97 kg mol^{-1}, polydispersity index = 1.12), and PS-P2VP (Polymer Source, M_n^{PS} = 130 kg mol^{-1}, M_n^{P2VP} = 135 kg mol^{-1}, polydispersity index = 1.30) in place of the PS-P4VP.

STEM and EDS images were obtained with a JEOL JEM-2010FEF(HR) transmission electron microscope operating at 200 keV. The untilted samples were observed after being embedded in epoxy and microtomed with diamond knife into 50 nm thick slices.

dx.doi.org/10.1021/mz300634p | *ACS Macro Lett.* 2013, 2, 284–287

SAXS measurements were performed at the BL33XU beamline of SPring-8. Wide-angle X-ray scattering patterns were collected on a Rigaku RINT-TTR (Cu Kα) operated at 40 kV and 50 mA. Thermal decomposition of the samples up to 1273 K was measured by a thermogravimetric analysis instrument (Rigaku, Thermo Plus) under a nitrogen atmosphere. The elemental analysis was carried out by inductively coupled plasma atomic emission spectrometry (Rigaku, CIROS-120 EOP).

■ ASSOCIATED CONTENT

Ⓢ Supporting Information

Experimental details, STEM images, EDS images, X-ray diffraction, and thermogravimetric analysis results. This material is available free of charge via the Internet at http://pubs.acs.org.

■ AUTHOR INFORMATION

Corresponding Author

*E-mail: wakayama@mosk.tytlabs.co.jp.

Notes

The authors declare no competing financial interest.

■ ACKNOWLEDGMENTS

The SAXS experiments were performed at the BL33XU beamline of SPring-8 with the approval of the Japan Synchrotron Radiation Research Institute (JASRI; Proposal Nos. 2011A7003 and 2011B7003).

■ REFERENCES

(1) Tsurumi, T.; Miyasou, T.; Ishibashi, Y.; Ohashi, N. *Jpn. J. Appl. Phys., Part 1* **1998**, *37* (9B), 5104.
(2) Dresselhaus, M. S.; Chen, G.; Tang, M. Y.; Yang, R. G.; Lee, H.; Wang, D. Z.; Ren, Z. F.; Fleurial, J. P.; Gogna, P. *Adv. Mater.* **2007**, *19*, 1043.
(3) Mizuno, F.; Hayashi, A.; Tadanaga, K.; Tatsumisago, M. *Adv. Mater.* **2005**, *17*, 918.
(4) Kneller, E. F.; Hawig, R. *IEEE Trans. Magn.* **1991**, *27*, 3588.
(5) Skomski, R.; Coey, J. M. D. *Phys. Rev. B* **1993**, *48*, 15812.
(6) Schrefl, T.; Kronmüller, H.; Fidler, J. *J. Magn. Magn. Mater.* **1993**, *127*, L273.
(7) Teranishi, T.; Wachi, A.; Kanehara, M.; Shoji, T.; Sakuma, N.; Nakaya, M. *J. Am. Chem. Soc.* **2008**, *130*, 4210.
(8) Kildishev, A. V.; Cai, W.; Chettiar, U. K.; Yuan, H. K.; Sarychev, A. K.; Drachev, V. P.; Shalaev, V. M. *J. Opt. Soc. Am. B* **2006**, *23*, 423.
(9) Nozawa, T.; Arakawa, Y. *Appl. Phys. Lett.* **2011**, *98* (17), 171108−1.
(10) Li, L.; Ma, R.; Ebina, Y.; Fukuda, K.; Takada, K.; Sasaki, T. *J. Am. Chem. Soc.* **2007**, *129*, 8000.
(11) Söderberg, H.; Odén, M. *J. Appl. Phys.* **2005**, *97*, 114327−1.
(12) Oshima, R.; Takata, A.; Shoji, Y.; Akahane, K.; Okada, Y. *Phys. E* **2010**, *42*, 2757.
(13) Lee, S. W.; Kumpfer, J. R.; Lin, P. A.; Gao, X. P. A.; Rowan, S. J.; Sankaran, R. M. *Macromolecules* **2012**, *45*, 8201.
(14) Dong, Q.; Li, G.; Ho, C. L.; Faisal, M.; Leung, C. W.; Pong, P. W. T.; Liu, K.; Tang, B. Z.; Manners, I.; Wong, W. Y. *Adv. Mater.* **2012**, *24*, 1034.
(15) Pai, R. A.; Humayun, R.; Schulberg, M. T.; Sengupta, A.; Sun, J. N.; Watkins, J. J. *Science* **2004**, *303*, 507.
(16) Yang, P.; Zhao, D.; Margolese, D. I.; Chmelka, B. F.; Stucky, G. D. *Chem. Mater.* **1999**, *11*, 2813.
(17) Warren, S. C.; Messina, L. C.; Slaughter, L. S.; Kamperman, M.; Zhou, Q.; Gruner, S. M.; DiSalvo, F. J.; Wiesner, U. *Science* **2008**, *320*, 1748.
(18) Templin, M.; Franck, A.; Chesne, A. D.; Leist, H.; Zhang, Y.; Ulrich, R.; Schadler, V.; Wiesner, U. *Science* **1997**, *278*, 1795.
(19) Garcia, C. B. W.; Zhang, Y. M.; Mahajan, S.; DiSalvo, F.; Wiesner, U. *J. Am. Chem. Soc.* **2003**, *125*, 13310.
(20) Kuila, B. K.; Rama, M. S.; Stamm, M. *Adv. Mater.* **2011**, *23*, 1797.
(21) Chen, A.; Komura, M.; Kamata, K.; Iyoda, T. *Adv. Mater.* **2008**, *20*, 763.
(22) Chai, J.; Wang, D.; Fan, X.; Buriak, J. M. *Nat. Nanotechnol.* **2008**, *320*, 1748.
(23) Lu, Q. L.; Kopley, T. E.; Moll, N.; Roitman, D.; Chamberlin, D.; Fu, Q.; Liu, J.; Russel, T. P.; Rider, D. A.; Manners, I.; Winnik, M. A. *Chem. Mater.* **2005**, *17*, 2227.
(24) Rider, D. A.; Liu, K.; Eloi, J. C.; Vanderark, L.; Yang, L.; Wang, J. Y.; Grozea, D.; Lu, Z. H.; Russel, T. P.; Manners, I. *ACS Nano* **2008**, *2*, 263.
(25) Aissou, K.; Fleury, G.; Pecastaings, T.; Alnasser, T.; Mornet, S.; Goglio, G.; Hadziioannou, G. *Langmuir* **2011**, *27*, 14481.
(26) Xu, C.; Ohno, K.; Ladmiral, V.; Milkie, D. E.; Kikkawa, J. M.; Composto, R. J. *Macromolecules* **2009**, *42*, 1219.
(27) Sohn, B. H.; Choi, J. M.; Yoo, S. I.; Yun, S. H.; Zin, W. C.; Jung, J. C.; Kanehara, M.; Hirata, T.; Teranishi, T. *J. Am. Chem. Soc.* **2003**, *125*, 6368.
(28) Meiner, J. C.; Quintel-Ritzi, A.; Mlynek, J.; Elbs, H.; Krausch, G. *Macromolecules* **1997**, *30*, 4945.
(29) Sakurai, S. *Polymer* **2008**, *49*, 2781.